

NUMERICAL STUDIES ON NOISE-SHIELDING EFFECTS OF A BLENDED-WING-BODY AIRCRAFT USING BOUNDARY ELEMENT METHOD

Hongyan Wang^{1,2}, Collin Tatenda Mutasa^{1,2} & Zhenli Chen^{1,2}

¹National Key Laboratory of Aircraft Configuration Design, Xi'an 710072, China ²School of Aeronautics, Northwestern Polytechnical University, Xi'an 710072, China

Abstract

Blended-Wing-Body (BWB) civil aircraft is an advanced configuration integrating the engines on the rear center-body, which has great potential on noise shielding by adopting Propulsion Airframe Aeroacoustics (PAA) effects. With the development of High-Bypass-Ratio (HBPR) engines, the jet noise will no longer be the most dominant component of engine noise sources, but the fan noise emerges. Although the center-body of a BWB can shield the forward radiated fan noise, the PAA effects still needs to be scrutinized in detail. The effects of noise frequency, nacelle, and engine position on the shielding are studied by using the fast multipole Boundary Element Method (BEM). The nacelle alone blocks the bulk of sound energy inside the nacelle and reduces the sound pressure outside the nacelle, which produces a noise reduction. The frequency also has a great impact on the noise shielding of BWB. The higher the frequency, the smaller the propagation angle of forward radiated noise, which decreases the noise shielding. However, the scattering effects on the BWB surface decay the energy. Thus, the diffraction on the leading and trailing edges is weakened, leading to the enhancement of the noise shielding underneath the center-body. Three configurations with different typical engine mounted positions are investigated via a defined synthetical method. The results indicate that BWB with the engines mounted on the rear upper surface produces the largest reduction on both forward and aft radiated noise with a value up to 5dB.

Keywords: Blended-Wing-Body, Propulsion Airframe Aeroacoustics Effects, Fan Noise Shielding, Fast Multipole Boundary Element Method

1. Introduction

With the rising of demand on travel by air, a large number of civil aircrafts is projected in the near future which can result in more severe noise and green-house gas emissions. Thus, the consideration of noise reduction becomes indispensable in civil aircraft design.

The potential of noise reduction is limited for the current tube-and-wing (TAW) configurations, hence new environmentally friendly configurations might be required to achieve ambitious noise-reduction goals for the next-generation aircraft. It is believed that the noise reduction potential of the engine is limited by the HBPR, and changing the aircraft configuration to one with favorable Propulsion Airframe Aeroacoustics (PAA) effects, specifically to replace the reflection with shielding of engine noise is a key to meet the low noise goals. PAA can not only reduce the noise sources that arise specifically from the integration of propulsion and airframe but also use the installation itself as a means to reduce noise[1]. Using the airframe to shield engine noise from ground is the most obvious, direct and promising way to reduce noise for unconventional aircraft, and it represents the main potential of noise reduction for unconventional aircraft[2].

National Aeronautics and Space Administration (NASA) of America and other organizations[3–5] have conducted extensive researches on the unconventional configurations, especially the Blended-Wing Body (BWB) with engines mounted on the rear upper surface. The adoption of the favorable

PAA effects has been recognized as the key of the low-noise design. The critical silent aircraft experimental design SAX-40 during the Silent Aircraft Initiative (SAI) yielded a noise reduction of 75 EPNdB cumulative to the Federal Aviation Administration (FAA) stage 4 noise certification regulation[6].

In the stage of conceptual design, PAA effects can be accurately predicted by performing experiments due to the heavy computationally intensive of the Computational Aeroacoutics (CAA) approach and the limited prediction methods of PAA effects for unconventional configurations. The experiments on PAA effects can be roughly divided into two parts. One is to increase the shielding area for the aft radiated fan noise and the jet noise by moving the engines upstream or by extending the trailing edge downstream[7–11]. The other is to adopt PAA, such as nozzle and pylon modifications, to reduce the level of jet noise sources or to move jet noise sources upstream to enhance the shielding[12–15].

Based on the extensive experimental data that contains hundreds of configuration types, noise sources, low-noise technologies and design parameters, the PAA effects have been accounted into Aircraft Noise Prediction Program 2 (ANOPP2). Aircraft system noise level of NASA HWB300-2009 was analyzed by Thomas.[1]. It was found that the PAA effects provided a noise reduction of 7.4 EP-NdB cumulative by just moving engines upstream three times of the fan nozzle diameter to that of the baseline. Guo[16] analyzed the aircraft-level noise of Boeing's BWB using the ANOPP2 that contains the assessment of Krueger slat. It was found that shielding of engine noise provided a reduction of about 7 EPNdB. Meanwhile, Guo proposed a new ranking order of various noise components, revealing that the engine noise sources are not the dominant ones due to both the low level of engine noise sources and the shielding by the airframe.

At the end of NASA Environmentally Responsible Aviation (ERA), the aircraft system noise of four different configurations and five passenger classes[17] were assessed by Thomas[18]. The HWB301, as compared to the TAW301, had a total noise reduction of 11.9 EPNdB by PAA as a result of replacing noise reflection with shielding. The HWB301-GTF with a group of newer low-noise approaches reaches a noise level of 50.9 EPNdB cumulative below Stage 4[19], very close to the NASA Far-Term noise goal. A total noise reduction of 10.5 EPNdB cumulative was achieved from the baseline to the low-noise HWB301-GTF. Among this, a noise reduction of 2.5 EPNdB cumulative was produced by the noise shielding. A TAW, a mid-fuselage nacelle (MFN) and a hybrid wing body (HWB) which were conceptually designed with the same technologies and mission requirements were assessed to demonstrate and to quantify the PAA effects from configuration change[17]. The noise analysis showed a total PAA effects of 10.7 EPNdB cumulative. That is, a noise reduction of 6.4 EPNdB for the HWB with shielding of engine noise while a noise increase of 4.3 EPNdB for the TAW[20].

Over the past two decades, most of the studies focused on the aircraft-level noise reduction of BWB by enhancing the shielding of jet noise using experiments and empirical methods. With the development of HBPR engines, the jet noise will no longer be the most dominant component of engine noise, but the fan noise emerges. However, few studies have been done to study the shielding of fan noise sources, especially using numerical methods. Although the center-body of a BWB can shield the forward radiated fan noise, the PAA effects still need to be scrutinized in detail.

In this paper, a fast multipole Boundary Element Method (BEM) is adopted to study the shielding effects of monopoles mounted inside the nacelles to model the engines on a BWB civil aircraft without freestream flow. The parameter studies of frequency, nacelle, and engine position on the noise shielding effects are performed. Moreover, the shielding of engine noise sources are presented in the form of contours for the sound field or along a line for a single monitoring point in previous studies which can not clearly quantify the shielding effects. A synthetical assessment on noise shielding of BWB is defined which has not been seen in the previous studies, and the shielding effects underneath the center-body of BWB are clearly demonstrated and quantified.

2. Numerical method and validation

2.1 Numerical method

The BEM is a semi-analytical method which is in the boundary integral equations (BIEs) formulation[21]. The conventional BIE (CBIE) of sound pressure for the scattering acoustic problem in 3D space can be written as

$$c(\mathbf{x})\phi(\mathbf{x}) = \int \left[G(\mathbf{x}, \mathbf{y}, \boldsymbol{\omega}) q(\mathbf{y}) - F(\mathbf{x}, \mathbf{y}, \boldsymbol{\omega}) \phi(\mathbf{y})\right] dS(\mathbf{y}) + \phi^{s}(\mathbf{x}), \forall \mathbf{x} \in S,$$
(1)

where $G(\mathbf{x}, \mathbf{y}, \boldsymbol{\omega})$ and $F(\mathbf{x}, \mathbf{y}, \boldsymbol{\omega})$ are the Green's function; $c(\mathbf{x}) = \frac{1}{2}$ if S is smooth around \mathbf{x} and $q = \frac{\partial \phi}{\partial n}$. ϕ^s is the term including all the source, and $\phi^s = Q_m G(\mathbf{x}, \mathbf{x_m}, \boldsymbol{\omega})$ with only monopoles are used in this work.

CBIE Eq. (1) could be used to solve the acoustic pressure on *S*. However, it has nonunique solutions at a set of fictitious eigenfrequencies associated with the resonate frequencies of the corresponding interior problems[22]. A remedy to this problem is to use the hypersingular BIE (HBIE) in conjunction with CBIE. HBIE is given by

$$\tilde{c}(\mathbf{x}) q(\mathbf{x}) = \int \left[K(\mathbf{x}, \mathbf{y}, \boldsymbol{\omega}) q(\mathbf{y}) - H(\mathbf{x}, \mathbf{y}, \boldsymbol{\omega}) \phi(\mathbf{y}) \right] dS(\mathbf{y}) + q^{s}(\mathbf{x}), \forall \mathbf{x} \in S,$$
(2)

where $K(\mathbf{x}, \mathbf{y}, \boldsymbol{\omega}) = \frac{\partial G(\mathbf{x}, \mathbf{y}, \boldsymbol{\omega})}{\partial n(\mathbf{x})}$ and $H(\mathbf{x}, \mathbf{y}, \boldsymbol{\omega}) = \frac{\partial F(\mathbf{x}, \mathbf{y}, \boldsymbol{\omega})}{\partial n(\mathbf{x})}$ are the Green's function. A linear combination of CBIE Eq. (1) and HBIE Eq. (2) which called Burton-Miller BIE formulation[22] is used to yield unique solutions for the exterior acoustic scattering problems in 3D space. Burton-Miller BIE is given by

$$CBIE + \beta HBIE = 0, (3)$$

where β is a coupling constant.

Once the value of ϕ is known on S, ϕ everywhere in the acoustic domain, E, could be calculated by

$$\phi(\mathbf{x}) = \int [G(\mathbf{x}, \mathbf{y}, \boldsymbol{\omega}) q(\mathbf{y}) - F(\mathbf{x}, \mathbf{y}, \boldsymbol{\omega}) \phi(\mathbf{y})] dS(\mathbf{y}) + \phi^{s}(\mathbf{x}), \forall \mathbf{x} \in E.$$
(4)

However, BEM lacks of efficiency on large-scale model simulation at high frequency. A fast multipole BEM of Liu[23] is adopted to speed up the simulations.

2.2 Validation of BEM method

A rectangular plate with dimensions of $5m \times 2m \times 0.0032m$ shown in Figure 1 is used to validate the fast multipole BEM. A unit strength monopole is placed 0.25m above the center of the plate. Experimental data of Ahtye[24] and numerical data of the Fast Scattering Code (FSC) using a thicker rectangular plate with a thickness of 0.07m[25] are used for validation.

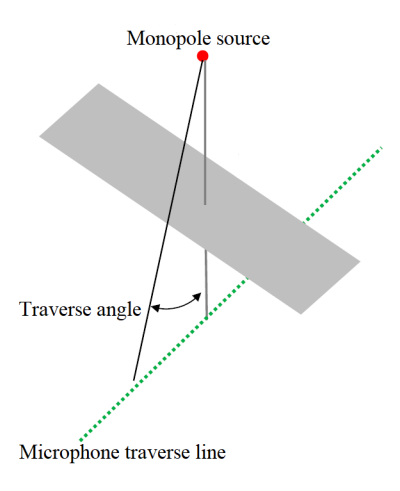
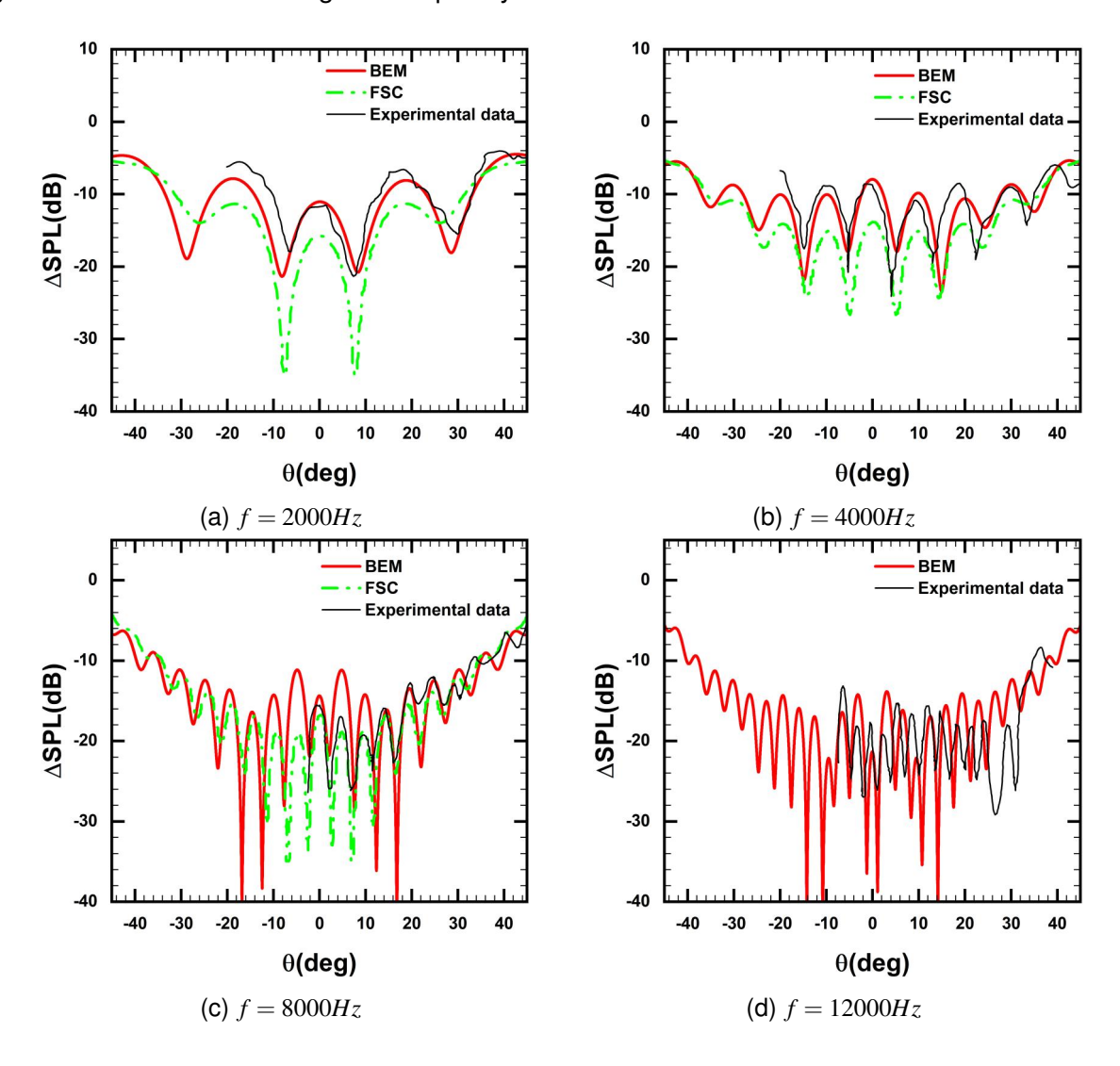


Figure 1 – Schematic of the rectangular plate problem.

A sound pressure level difference, ΔSPL , defined in Eq. (5) is used to evaluate the shielding effects.

$$\Delta SPL = 20log_{10} \left(\frac{p_{shielded}}{p_{unshielded}} \right) \tag{5}$$

Comparisons between numerical and experimental data at a series of frequencies are shown in Figure 2. The data could be slightly different from the stated frequency which had been presented nondimensional and the speed of sound was not reported in the experiment. Besides, the highest frequency of the FSC is 8000Hz, which is lower than the highest frequency of the experimental data and the simulations here. Therefore, the comparisons of ΔSPL between FSC and BEM are performed just up to 8000Hz. As shown in Figure 2, the sound magnitude and directivity are captured well, that is, the peaks and valleys of the sound waves are generally coincident by the simulations adopting BEM method, and the results of the BEM are better than that of FSC. At the frequencies lower than 20000Hz, the BEM results are in good agreement with experimental data with a difference of less than 3dB. However, the discrepancy between experiment and the simulation becomes large with the magnitude of 6.5-9dB at the highest frequency of 20000Hz.



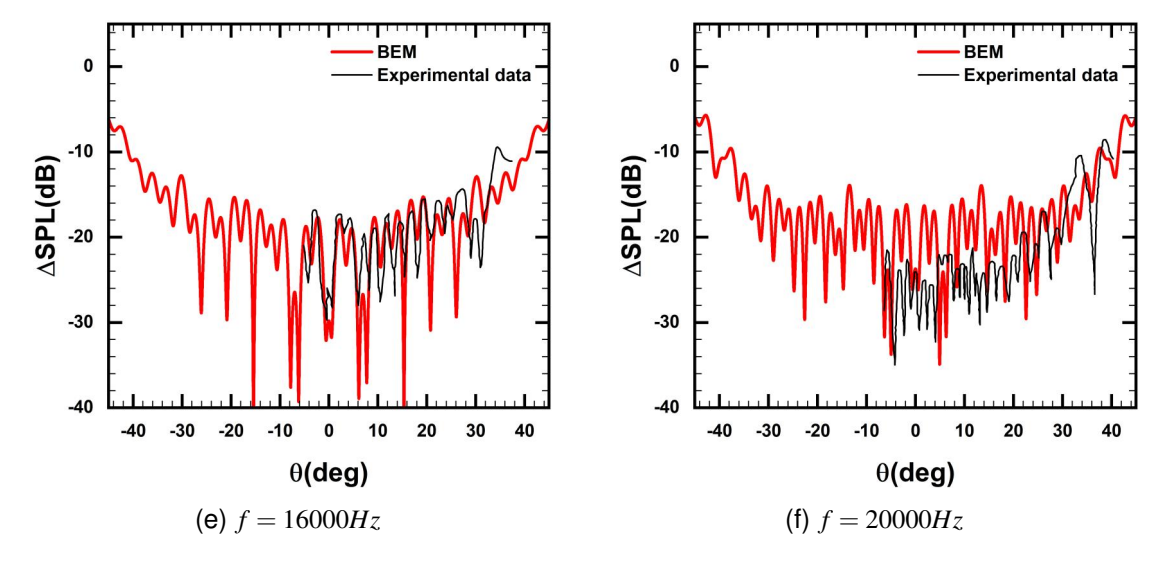


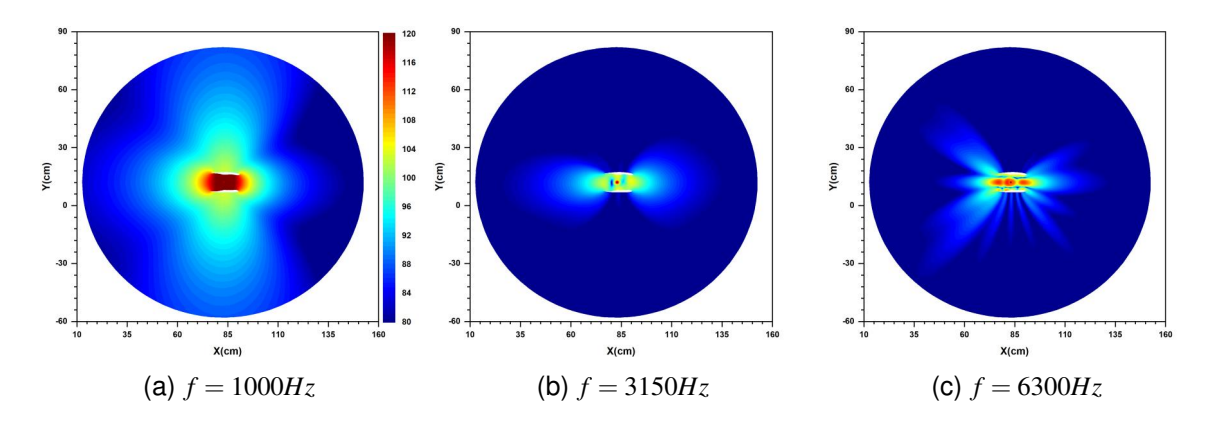
Figure 2 – Comparisons between experimental data and simulations.

3. Shielding Effects of BWB aircraft

To reduce the computational cost, acoustic simulations of a 3% scaled SWB-300 aircraft[26, 27] with engines mounted on the upper rear surface without freestream flow are carried out. The effects of a range of parameters including frequency, nacelle and engine position on engine noise shielding are considered.

3.1 Shielding effects of nacelles

Numerical simulations of a single nacelle is conducted to study the effects of the nacelle on noise radiation patterns of one monopole inside the nacelle. Simulated radiation patterns of a nacelle at different frequencies are presented in Figure 3. The noise diffracts at the nacelle edges and then envelops the nacelle because the wavelength and nacelle length are comparable at f=1000Hz, as shown in Figure 3(a). As the frequency increases further, the diffraction strength around the edge decreases. It is clearly observed from Figure 3(b) that one lobe radiated outside the nacelle at the frequency of 3150Hz. There are three radial lobes that are distinguished within the nacelle at f=6300Hz, and the bulk of energy coalesces into one lobe that radiates through the both inlet and outlet close to the axis of the nacelle. As the frequency increases further, the patterns of radiated noise become more complex. For the higher frequency cases, more lobes are cut on inside the nacelle. At frequency 12500Hz, as shown in Figure 3(f), most energy is trapped inside the nacelle and the energy radiating outside attenuates because the wavelength is far smaller than the diameter of nacelle, and the noise is scattered on the wall of nacelle resulting in rapid energy decay.



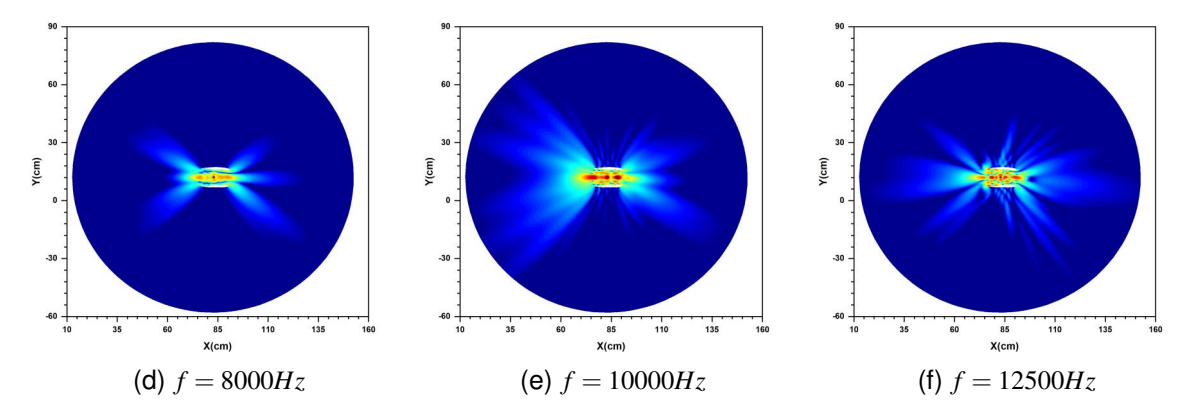


Figure 3 – The SPL contours of a nacelle with one monopole inside at different frequencies.

The ΔSPL defined in Eq. 5 is used to quantify the shielding effects of two nacelles with one monopole placed in each of them. The $\Delta SPLs$ of two nacelles at a series of center frequencies of one-third-octave bands are shown in Figure 4 with the negative values represent the SPLs decrease. These results present an "unwrapped" view of a cylinder field which has a diameter of 2m. The X-axis represents the longitudinal positions along the body axis of the configuration. The vertical axis represents the circumferential direction from 0° to 360° with $\theta=0^{\circ}\sim90^{\circ}$ and $\theta=270^{\circ}\sim360^{\circ}$ representing the sound field underneath the configuration. At frequency f=1000~Hz, as shown in Figure 4(a), there is little noise shielding effect around the nacelles due to the strong diffraction around the nacelles edges. As the frequency increases, it is found that there is an obvious shadow zone located on the side of the nacelles.

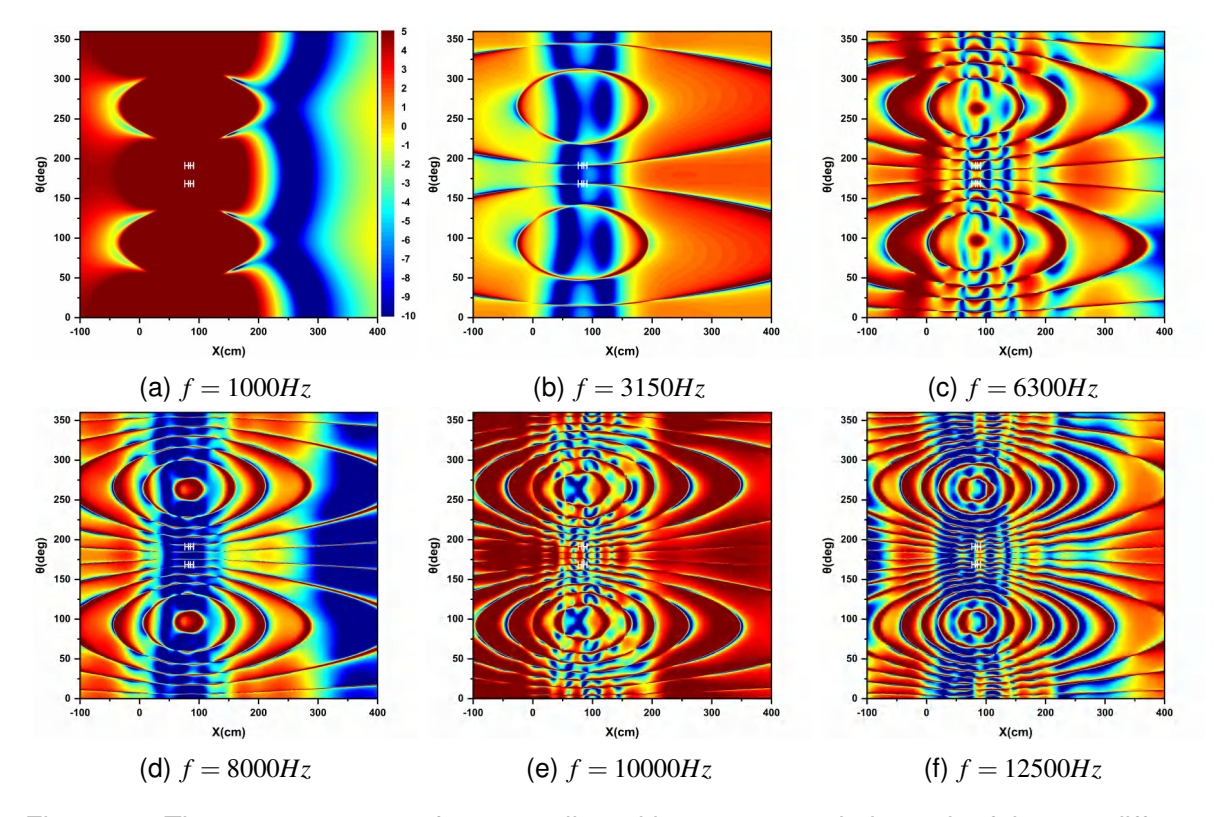


Figure 4 – The ΔSPL contours of two nacelles with one monopole in each of them at different frequencies.

3.2 The installation effects of baseline configuration

The installation effects are studied further with one monopole positioned on the shaft in each nacelle of both engines. Comparisons of the *SPLs* at different frequencies on the vertical symmetric plane of the nacelle are shown in Figure 5. It is found that the noise scattered on the BWB changes the direction around both the inlet and outlet of the nacelles. The propagation angle of forward radiated

noise decreases when the frequency increases, which enhances the SPL in front of the nacelle. The diffraction at the trailing edge of the center-body is decreased when the frequency increases. When the frequency increases to 8000Hz and above, as the wavelength is smaller than the nacelle diameter, the diffraction strength around the nacelle edges attenuates, and the scattering effects on the wall of nacelles result in rapid energy decay outside the nacelles. The sound energy is further dissipated under the scattering effects on the surface of BWB, thus the diffraction energy on the leading and trailing edges decays which decreases the SPL underneath the BWB.

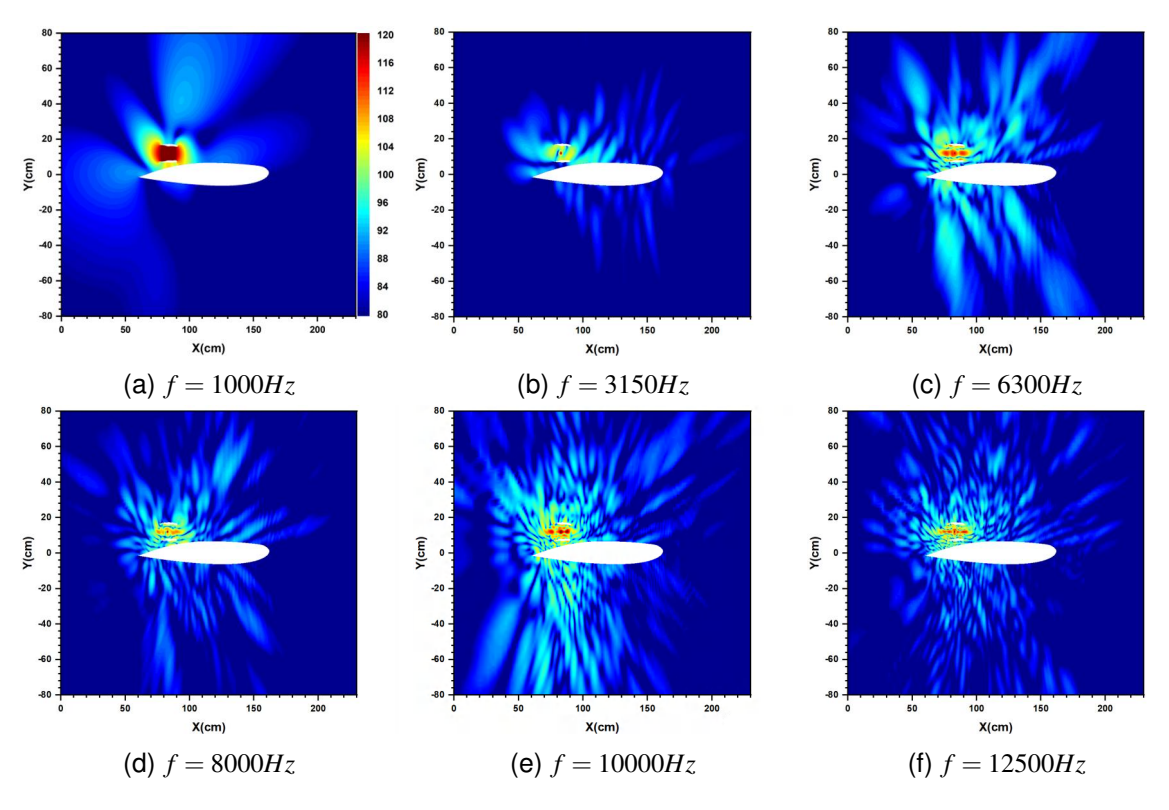
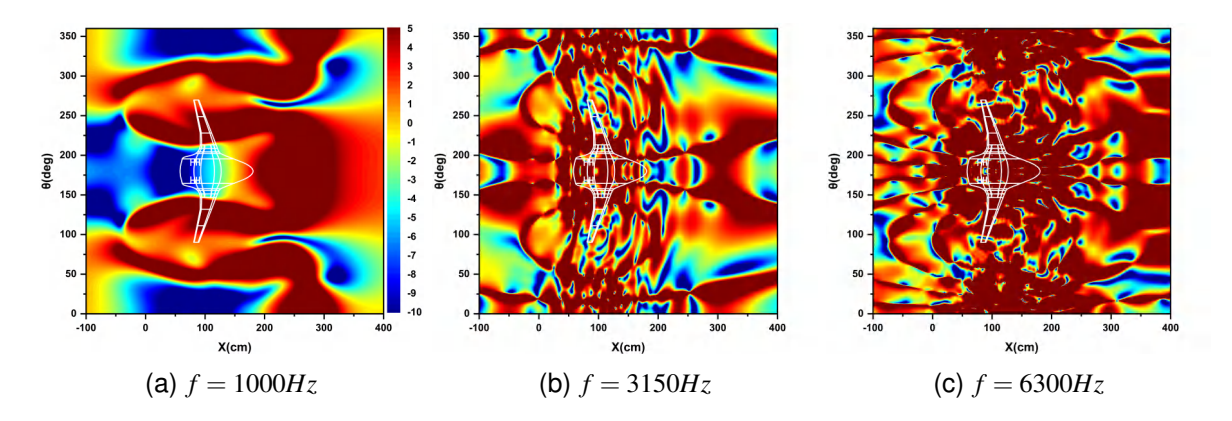


Figure 5 – Comparisons of *SPL* contours at different frequencies on the vertical symmetric plane of the nacelle.

A key objective of this study is to figure out the noise shielding effects of the airframe. The ΔSPL is defined as the difference of SPL between nacelles with/without BWB to quantify the shielding effects. The installation effects at different center frequencies of 1/3 octave bands are shown in Figure 6. It is clearly observed that the existence of the center body further blocks the sound wave for both forward and rearward radiated noise from propagating underneath the center body. The maximum local shielding can be up to 50dB.



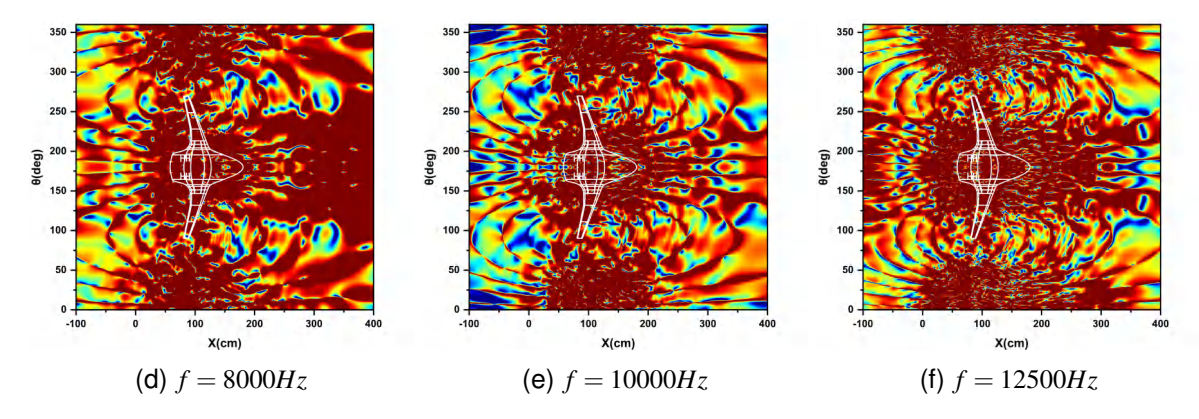


Figure 6 – Comparisons of ΔSPL contours of BWB installing two nacelles having monopoles at different frequencies.

Comparisons of ΔSPL at different frequencies at $\theta=360^\circ$ along the body axis underneath the BWB are shown in Figure 7. It is notable that the BWB provides noise shielding for both forward and rearward radiated noise. it is found that the noise shielding for the aft radiated noise are better than that of forward radiated noise. For the aft radiated fan noise, the magnitude of noise reduction due to noise shielding is up to 20dB while a reduction up to 10dB for the forward radiated fan noise.

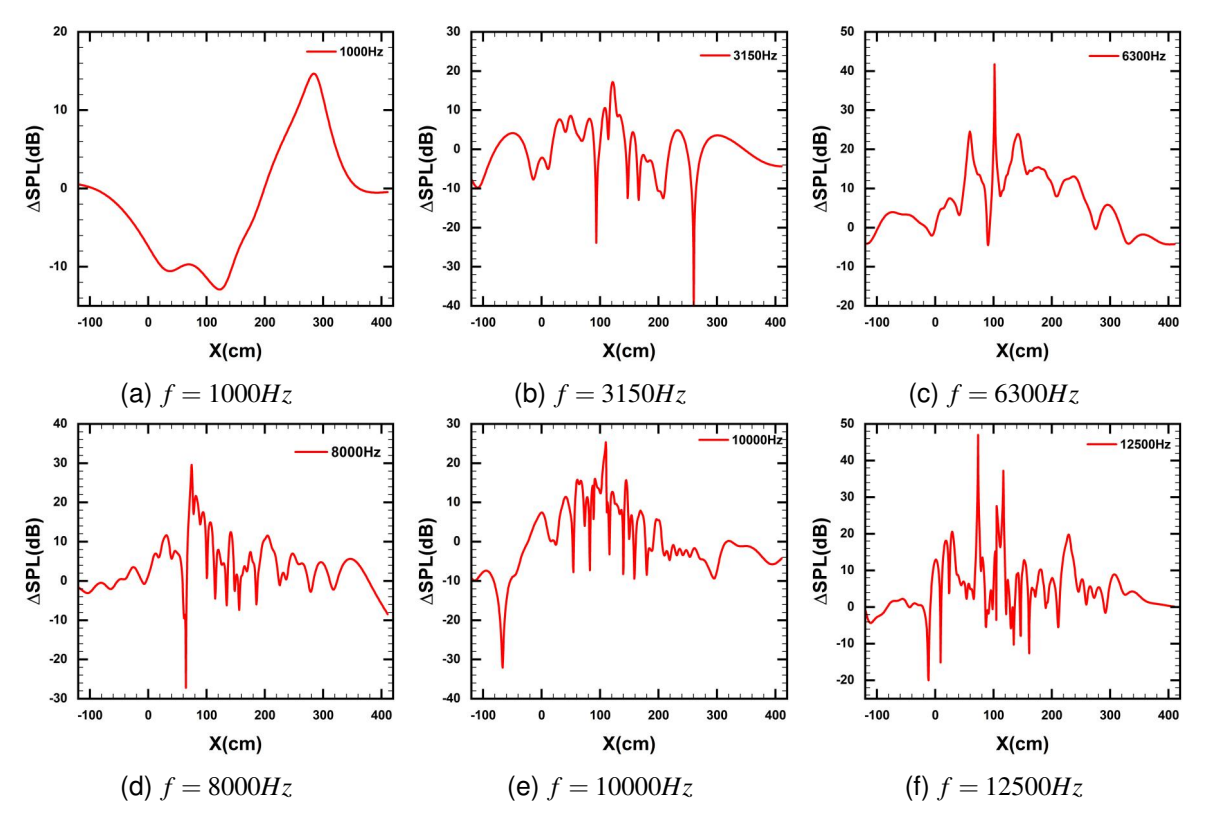


Figure 7 – Comparisons of $\triangle SPL$ contours of the baseline configuration at $\theta=360^{\circ}$ along the body axis at different frequencies .

3.3 Effects of engine locations on noise shielding

It is known that the shielding effects are sensitive to the engine positions. Three typical engine positions are selected to study the effects of engine installation on the PAA effects. The positions are over the rear center body, over the wing at the trailing edge, and under the wing near the leading edge, as shown in Figure 8, where *D* is the diameter of the nacelle exit.

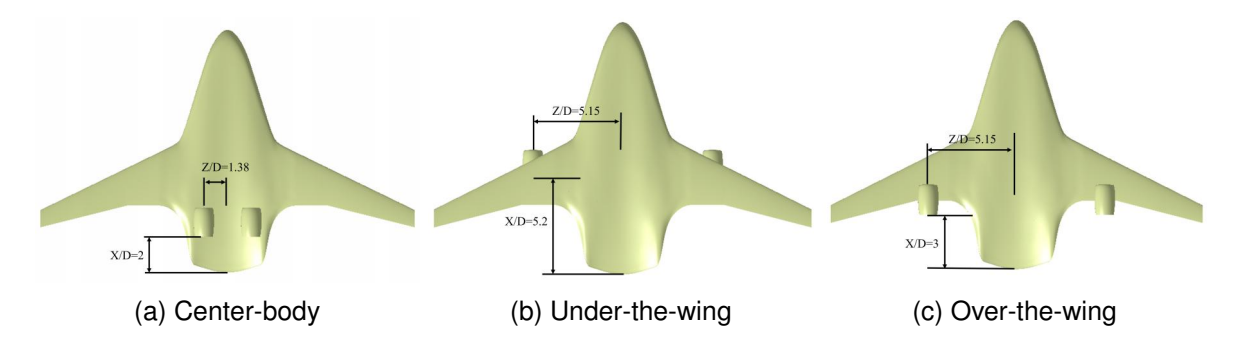
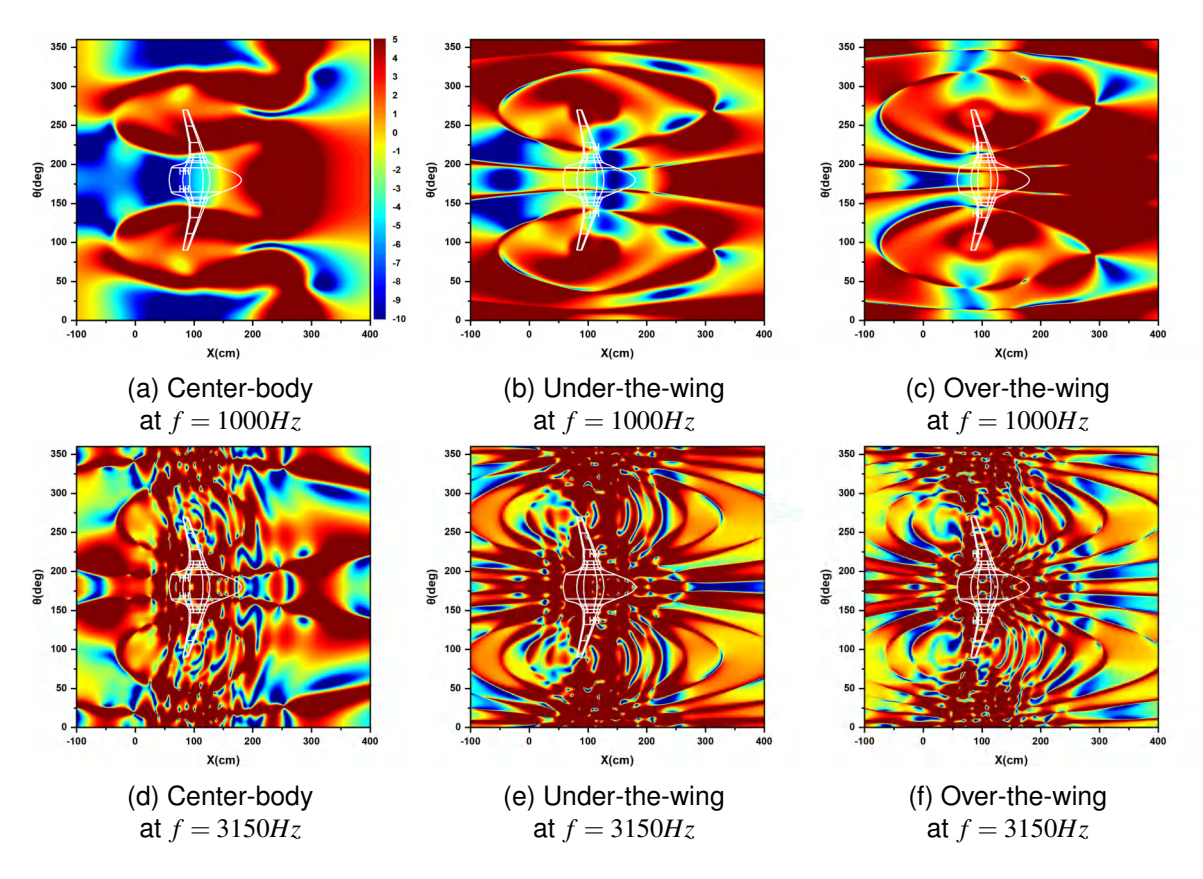


Figure 8 – Positions of engines mounted on the airframe.

One monopole is mounted inside each nacelle of two engines to model engines' noise sources. The noise scattering and diffraction patterns for over- and under-the-wing positions are much different from that of the center-body configuration, as shown in Figure 9. At the low frequencies of 1000Hz and 3150Hz, the shielding effects of the center-body are much better than the others. Under-the-wing aircraft does not provide shielding effects underneath the airframe due to the reflections. The configuration with engines mounted over the wing reduces the reflection of the sound waves and has some shielding, and produces a noise reduction of forward radiated noise. As the frequency increases, the shielding effects of forward radiated noise underneath the airframe for the center body mounted engines are still better than that of over- and under-the-wing positions.



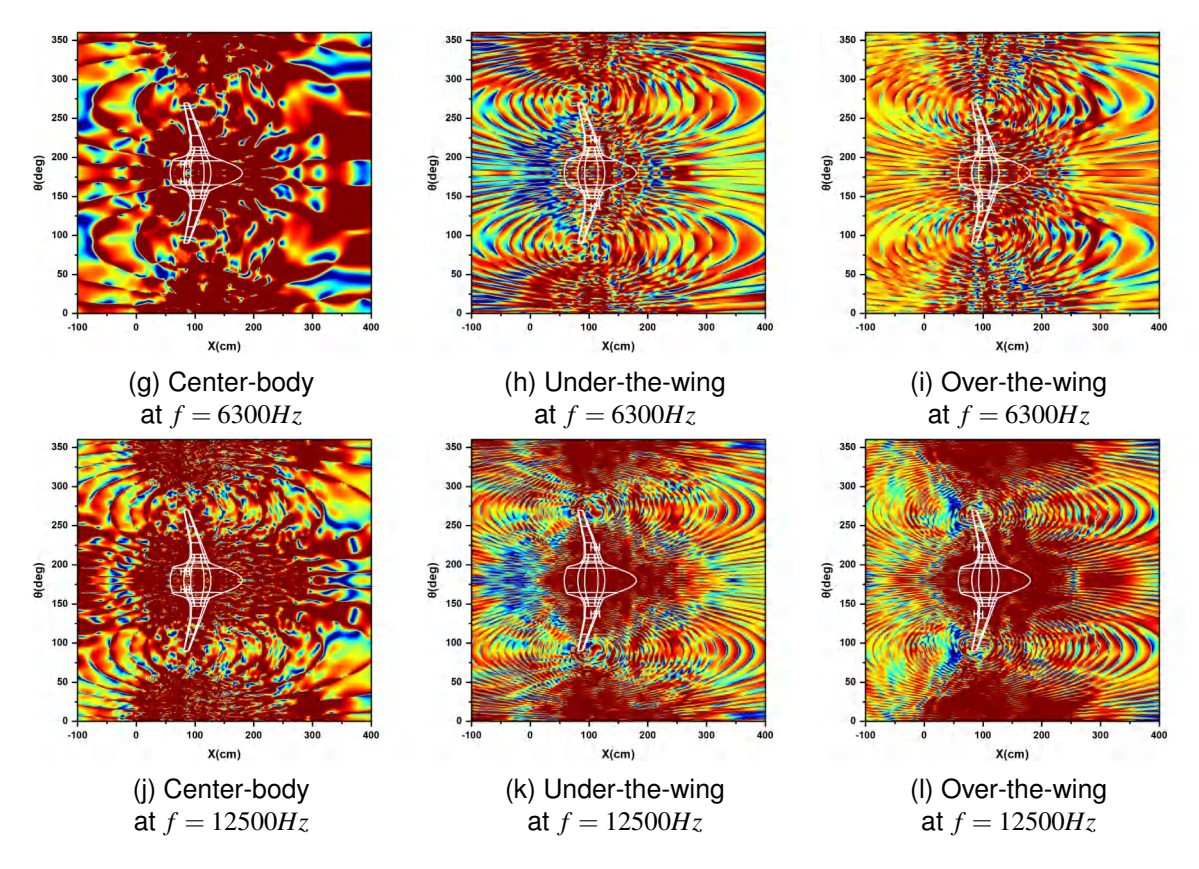


Figure 9 – The effects of different installation positions of engines on shielding at different frequencies.

The engine fan noise shielding effect is difficult to quantify in the form of ΔSPL contours which is the most common method used in previous studies due to the complex small structures especially at high frequencies. To quantitatively and synthetically analyze the noise shielding of different engine positions, a mean sound pressure within $\theta = 0^{\circ} \sim 90^{\circ}$ and $\theta = 270^{\circ} \sim 360^{\circ}$ is defined in Eq. (6) and Eq. (7) for the cases with and without BWB, respectively. Then a mean sound pressure level difference over the lower half cylinder under the center-body is defined in Eq. (8).

$$\overline{p_s(x)} = \sqrt{\frac{\int_0^{\frac{\pi}{2}} p_s^2(x) d\theta + \int_{\frac{3\pi}{2}}^{\pi} p_s^2(x) d\theta}{\pi}},$$
(6)

$$\overline{p_{sa}(x)} = \sqrt{\frac{\int_0^{\frac{\pi}{2}} p_{sa}^2(x) d\theta + \int_{\frac{3\pi}{2}}^{\pi} p_{sa}^2(x) d\theta}{\pi}},$$

$$\overline{\Delta SPL}(x) = 20 \log_{10} \left(\frac{\overline{p_s(x)}}{\overline{p_{sa}(x)}}\right),$$
(8)

$$\overline{\Delta SPL}(x) = 20\log_{10}\left(\frac{\overline{p_s(x)}}{\overline{p_{sa}(x)}}\right),\tag{8}$$

where p_s and p_{sa} are the sound pressure with and without BWB, respectively. The $\overline{\Delta SPL}s$ of three different engine positions are compared in Figure 10. It is clear that the configuration with engines mounted on the center body has the best shielding with a maximum value of 5dB while the under-thewing configuration does not provide noise shielding effects because the reflections of the fuselage which enhance the sound pressure underneath the center body. The over-the-wing configuration provides some shielding with the value up to 1dB due to the shielding effect of the wing instead of the reflection. However, the shielding at f = 6300Hz is much different, as shown in Figure 10(c). This may be attributed to the strong diffraction around the leading and trailing edges as the propagation angle of forward radiated noise decreases, as shown in Figure 5(c).

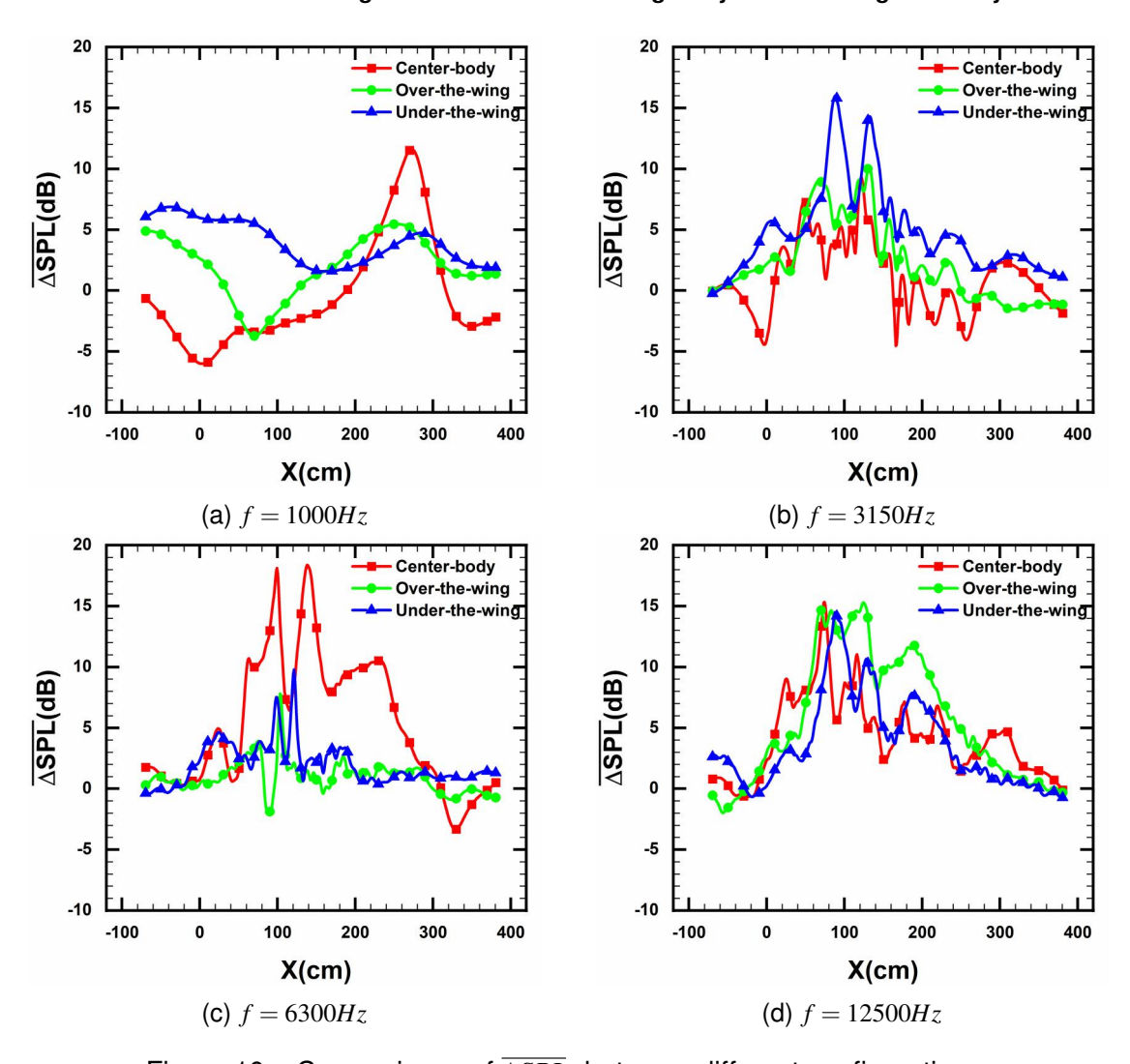


Figure 10 – Comparisons of $\overline{\Delta SPLs}$ between different configurations.

4. Conclusion

Engine fan noise is the most dominant component of engine noise sources with the increasing HBPR of turbofan engines. BWB with podded engines has great potential to reduce the fan noise by shielding provided by the center-body. In this paper, a fast multipole BEM is adopted to study the effects of several key design parameters including nacelle, frequency and engine position on the noise shielding.

Shielding results indicate that the nacelles can provide some noise shielding while strong diffractions at the edges of the nacelles at lower frequencies enhance the *SPL* in front and rear of the nacelles. At high frequencies, the radiated energy decays because of the scattering effects on the wall of nacelles.

The shielding effects of the baseline BWB configuration is analyzed. The BWB provides a shielding with a value up to 20dB at some specific frequencies. The propagation angle of forward radiated noise decreases when the frequency increases, which enhances the *SPL* in front of the nacelle. However, the *SPL* underneath the BWB is reduced due to the energy attenuation by the scattering effects at high frequencies.

A new mean *SPL* shielding is defined to analyze the complex shielding patterns of three configurations with different engine mounting positions. The results show that the configuration with engines on the rear body is best for noise shielding. The engines mounted on the rear upper surface produce the largest noise reduction with a magnitude up to 5dB while the engines mounted under the wing does not provide noise shielding.

5. Contact Author Email Address

zhenlichen@nwpu.edu.cn

6. Acknowledgements

This work was supported partially by the Fundamental Research Funds for the Central Universities (No.3102019JC009)

7. Copyright Statement

The authors confirm that they, and/or their company or organization, hold copyright on all of the original material included in this paper. The authors also confirm that they have obtained permission, from the copyright holder of any third party material included in this paper, to publish it as part of their paper. The authors confirm that they give permission, or have obtained permission from the copyright holder of this paper, for the publication and distribution of this paper as part of the ICAS proceedings or as individual off-prints from the proceedings.

References

- [1] Thomas RH, Burley CL, Olson ED. Hybrid wing body aircraft system noise assessment with propulsion airframe aeroacoustic experiments. *International Journal of Aeroacoustics*, Vol.11, No.3-4, pp 369-409, 2012.
- [2] Hill GA, Brown SA, Geiselhart KA, et al. Integration of propulsion-airframe-Aeroacoustic technologies and design concepts for a quiet blended-wing-body transport. *AIAA 4th Aviation Technology, Integration and Operations (ATIO) Forum*, 2004: 6403.
- [3] Ostrikov NN, Denisov SL. Airframe shielding of noncompact aviation noise sources: theory and experiment. *21st AIAA/CEAS aeroacoustics conference*, 2015: 2691.
- [4] Pieren R, Le Griffon I, Bertsch L, et al. Perception-based noise assessment of a future blended wing body aircraft concept using synthesized flyovers in an acoustic VR environment—The ARTEM study. Aerospace Science and Technology, Vol.144, pp 108786, 2024.
- [5] Wienke F, Bertsch L, Blinstrub J, et al. System noise assessment of conceptual tube-and-wing and blended-wing-body aircraft designs. *AIAA Aviation 2023 Forum*,2023:4170.
- [6] Hileman J, Spakovszky Z, Drela M, et al. Airframe design for "silent aircraft". 45th AIAA Aerospace Sciences Meeting and Exhibit, 2007:453.
- [7] Clark L, Gerhold C. Inlet noise reduction by shielding for the blended-wing-body airplane. *5th AIAA/CEAS Aeroacoustics Conference and Exhibit* 1999: 1937.
- [8] Reimann C, Tinetti A, Dunn M. Noise scattering by the blended wing body airplane: measurements and prediction. *12th AIAA/CEAS Aeroacoustics Conference*, 2006: 2464.
- [9] Hutcheson FV, Brooks TF, Burley CL, et al. Shielding of turbomachinery broadband noise by a hybrid wing body aircraft configuration. 20th AIAA/CEAS Aeroacoustics Conference, pp 2624, 2014.
- [10] Truong AD, Papamoschou D. Experimental simulation of ducted fan acoustics at very small scale. *52nd Aerospace Sciences Meeting*, 2014:0718.
- [11] Guo YP, Thomas RH. Experimental study on open rotor noise shielding by hybrid-wing-body aircraft. *AIAA Journal*, Vol.54, No.1, pp 242-253, 2016.
- [12] Czech MJ, Thomas RH, Elkoby R. Propulsion airframe aeroacoustic integration effects for a hybrid wing body aircraft configuration. *International Journal of Aeroacoustics*, Vol.11, No.3-4, 2012.
- [13] Papamoschou D, Mayoral S. Jet noise shielding for advanced hybrid wing-body configuration. 49th AIAA Aerospace Sciences Meeting including the New Horizons Forum and Aerospace Exposition. 2011: 912.

Numerical Studies on Noise-shielding Effects of a Blended-Wing-Body Aircraft Using Boundary Element Method

- [14] Papamoschou D, Mayoral S. Jet noise shielding for advanced hybrid wing-body configuration. 49th AIAA Aerospace Sciences Meeting including the New Horizons Forum and Aerospace Exposition, 2011:912.
- [15] Doty MJ, Brooks TF, Burley CL, et al. Jet noise shielding provided by a hybrid wing body aircraft. 20th AIAA/CEAS aeroacoustics conference, 2014:2625.
- [16] Guo YP, Burley CL, Thomas RH. On noise assessment for blended wing body Aircraft. *52nd Aerospace Sciences Meeting*, 2014: 0365.
- [17] Nickol CL, Haller WJ. Assessment of the performance potential of advanced subsonic transport concepts for NASA's Environmentally Responsible Aviation Project. *AIAA Paper*, 2016-1030.
- [18] Thomas RH, Burley CL, Nickol CL. Assessment of the noise reduction potential of advanced subsonic transport concepts for NASA's Environmentally Responsible Aviation Project. *54th AIAA Aerospace Sciences Meeting*, 2016:0863.
- [19] Thomas RH, Guo YP, Berton JJ, Fernandez H. Aircraft noise reduction technology roadmap toward achieving the NASA 2035 Goal. 23rd AIAA/CEAS aeroacoustics conference, 2017:3193.
- [20] June J, Clark I, Thomas RH, Guo YP. Far term noise reduction technology roadmap for a large twin-aisle tube-and-wing subsonic transport. *25th AIAA/CEAS Aeroacoustics Conference*, 2019:2428.
- [21] Nishimura N. Fast multipole accelerated boundary integral equation methods. *Applied mechanics reviews*, Vol.55, No.4, pp 299-324, 2002.
- [22] Burton AJ, Miller GF. The application of integral equation methods to the numerical solution of some exterior boundary-value problems. *Proceedings of the Royal Society of London*. Series A, 323, No.1553, pp 201-210, 1971.
- [23] Liu YJ. Fast multipole boundary element method: theory and applications in engineering. Cambridge university press, 2009.
- [24] Ahtye WF, McCulley G. Evaluation of approximate methods for the prediction of noise shielding by airframe components. NASA Technical Paper 1004, 1980
- [25] Tinetti AF, Dunn MH. The fast scattering (FSC) validation studies and program guidelines. *Tech*, Rep.NASA/CR-2011-217158
- [26] Zhang MH, Chen ZL and Zhang BQ. A conceptual design platform for blended wing-body transports. 30th Congress of the International Council of the Aeronautical Science. 2016 Daejeon; ICAS: 2016.
- [27] Gu WT, Chen ZL and Zhang BQ. Physically-based multidisciplinary design optimization framework coupling airframe and propulsion. 30thCongress of the International Council of the Aeronautical Science. 2016 Daejeon; ICAS: 2016.